WD40 domain of Apc1 is critical for the coactivator-induced allosteric transition that stimulates APC/C catalytic activity

Qiuhong Li[a,b], Leifu Chang[a], Shintaro Aibara[a,1], Jing Yang[a], Ziguo Zhang[a], and David Barford[a,2]

[a]Medical Research Council Laboratory of Molecular Biology, Cambridge CB2 0QH, United Kingdom; and [b]Section of Structural Biology, Chester Beatty Laboratories, Institute of Cancer Research, London SW3 6JB, United Kingdom

Edited by Avram Hershko, Technion Israel Institute of Technology, Haifa, Israel, and approved July 21, 2016 (received for review May 4, 2016)

The anaphase-promoting complex/cyclosome (APC/C) is a large multimeric cullin–RING E3 ubiquitin ligase that orchestrates cell-cycle progression by targeting cell-cycle regulatory proteins for destruction via the ubiquitin proteasome system. The APC/C assembly comprises two scaffolding subcomplexes: the platform and the TPR lobe that together coordinate the juxtaposition of the catalytic and substrate-recognition modules. The platform comprises APC/C subunits Apc1, Apc4, Apc5, and Apc15. Although the role of Apc1 as an APC/C scaffolding subunit has been characterized, its specific functions in contributing toward APC/C catalytic activity are not fully understood. Here, we report the crystal structure of the N-terminal domain of human Apc1 (Apc1N) determined at 2.2-Å resolution and provide an atomic-resolution description of the architecture of its WD40 (WD40 repeat) domain ($Apc1^{WD40}$). To understand how $Apc1^{WD40}$ contributes to APC/C activity, a mutant form of the APC/C with $Apc1^{WD40}$ deleted was generated and evaluated biochemically and structurally. We found that the deletion of $Apc1^{WD40}$ abolished the UbcH10-dependent ubiquitination of APC/C substrates without impairing the Ube2S-dependent ubiquitin chain elongation activity. A cryo-EM structure of an APC/C–Cdh1 complex with $Apc1^{WD40}$ deleted showed that the mutant APC/C is locked into an inactive conformation in which the UbcH10-binding site of the catalytic module is inaccessible. Additionally, an EM density for Apc15 is not visible. Our data show that $Apc1^{WD40}$ is required to mediate the coactivator-induced conformational change of the APC/C that is responsible for stimulating APC/C catalytic activity by promoting UbcH10 binding. In contrast, Ube2S activity toward APC/C substrates is not dependent on the initiation-competent conformation of the APC/C.

APC/C | ubiquitination | cell cycle | UbcH10 | Ube2S

The eukaryotic cell cycle is controlled by oscillations in the activities of key regulatory proteins through the interplay of reversible protein phosphorylation and irreversible ubiquitin-dependent proteolysis (1–3). By ubiquitinating essential cell-cycle proteins, the anaphase-promoting complex/cyclosome (APC/C) is the crucial RING E3 ubiquitin ligase that controls accurate sister chromatid segregation, cytokinesis, and the initiation of chromosome replication (4–9). The APC/C and a second cullin–RING E3 ligase, the Skp1–Cul1–F-box protein (SCF), coordinate cell-cycle regulation and are important players in cancer biogenesis (10).

APC/C activity is controlled by its association with one of two coactivator subunits (either Cdc20 or Cdh1) that function to specify substrate recognition and stimulate ubiquitin transfer reactions (11–14). The mitotic coactivator Cdc20 preferentially binds to hyperphosphorylated APC/C, whereas Cdh1 also binds to unphosphorylated APC/C. Coactivators enhance vertebrate APC/C catalytic activity by increasing its affinity for the priming E2 UbcH10 (also known as "Ube2C") (12), whereas in budding yeast APC/C coactivators enhance E2 catalytic efficiency (13). The APC/C is a multisubunit E3 ligase composed of 15 different proteins (12). Five are tetratricopeptide repeat (TPR) proteins, four of which (Apc3, Apc6, Apc7, and Apc8) form structurally related homodimers. Apc12, Apc13, and Apc16 are TPR accessory subunits. Apc1 is the largest scaffolding subunit (molecular mass ∼200 kDa) (15). Its proteasome cyclosome (PC) domain shares the same PC repeat architecture as the Rpn1 and Rpn2 subunits of the 19S proteasome (16). The N-terminal region of Apc1 (Apc1N) is rich in β-strands and possesses a multitude of regulatory phosphorylation sites (17, 18). The APC/C catalytic module composed of Apc2 and Apc11 recruits canonical E2s (UbcH10 and UbcH5 in vertebrates, Ubc1 and Ubc4 in budding yeast) to catalyze substrate ubiquitination (19, 20). Apc2 is a cullin domain protein that interacts with the RING domain subunit Apc11. Apc10 and the coactivators are responsible for APC/C substrate recruitment. Apc15 is required for Cdc20 autoubiquitination in the context of the mitotic checkpoint complex (MCC), thereby regulating APC/C–MCC disassembly (21–23).

In human APC/C, UbcH10 and Ube2S synthesize polyubiquitin chains through a sequential mechanism. The association of UbcH10 with the RING domain of Apc11 ($Apc11^{RING}$) and Apc2's winged-helix B domain ($Apc2^{WHB}$) initiates ubiquitin-chain formation (19, 20, 24–26). Ube2S, on the other hand, is responsible for ubiquitin-chain extension and specifically assembles Lys11-linked ubiquitin chains on substrates targeted by the APC/C (14, 25, 27–30). In vertebrates, the RING domain of Apc11 is repurposed to

Significance

The anaphase-promoting complex/cyclosome (APC/C) is a large E3 ubiquitin ligase that controls progression through mitosis and entry into G1. Its capacity to recognize and ubiquitinate substrates is dependent on coactivator subunits that interact with substrate degrons and promote a conformational change of the APC/C to increase its affinity for the priming E2 UbcH10. We show that the WD40 domain of anaphase-promoting complex subunit 1 (Apc1) is required for communicating the conformational change initiated by the binding of coactivator to the catalytic module. In contrast to UbcH10, binding of the elongating E2 Ube2S and its APC/C-stimulated activity does not require the active state of the APC/C. The work raises the possibility that conformational changes of the Apc1 WD40 domain may play a role in regulating UbcH10 binding to the APC/C.

Author contributions: Q.L. and D.B. designed research; Q.L., L.C., S.A., J.Y., Z.Z. and D.B. performed research; Q.L., L.C., S.A., and D.B. analyzed data; and Q.L. and D.B. wrote the paper.

The authors declare no conflict of interest.

This article is a PNAS Direct Submission.

Data deposition: Protein coordinates of $Apc1^{WD40}$ have been deposited with the Research Collaboratory for Structural Bioinformatics (RCSB) Protein Data Bank (RCSB PDB ID code 5LGG). EM maps have been deposited with the Electron Microscopy Data Bank (EM-DB) [accession codes EMD-4047 (ternary APC/$C^{\Delta Apc1-WD40}$–Cdh1–Hsl1 complex) and EMD-4048 (apo APC/$C^{\Delta Apc1-WD40}$)].

[1]Present address: Science for Life Laboratory, 171 65 Solna, Stockholm, Sweden.

[2]To whom correspondence should be addressed. Email: dbarford@mrc-lmb.cam.ac.uk.

This article contains supporting information online at www.pnas.org/lookup/suppl/doi:10.1073/pnas.1607147113/-/DCSupplemental.

position the acceptor ubiquitin, conjugated to an APC/C substrate, for modification by Ube2S (14, 30, 31). UbcH10 and Ube2S together build branched ubiquitin chains on APC/C substrates, and these chains are recognized more efficiently by the proteasome (32). In budding yeast, APC/C modifies substrates with Lys48-linked ubiquitin chains. The E2 Ubc4 initiates the ubiquitin chain synthesis, whereas Ubc1 extends the Lys48-linked ubiquitin chains (33, 34).

Previous cryo-EM studies showed that Cdh1 association with the APC/C promotes substantial conformational changes in the catalytic module and the neighboring platform subunits Apc1, Apc4, and Apc5 (12). This change in conformation exposes the UbcH10-binding site of the catalytic module, enhancing UbcH10 association and thereby stimulating APC/C E3 ligase activity (12, 19). Here, we combined biochemical methods, X-ray crystallography, and single-particle EM to study the structure of Apc1N and to examine its functions in vitro. We demonstrate that Apc1N is essential for APC/C catalytic activity because it is required to mediate the coactivator-induced conformational changes necessary for UbcH10 to engage the APC/C catalytic module.

Results

Apc1N Comprises a WD40 β-Propeller Domain. The domain architecture of full-length Apc1 is shown in Fig. 1*A*. Apc1N is followed by the middle domain (Mid-N), a PC domain, and a C-terminal domain (Mid-C) that coalesces with Mid-N to form $Apc1^{Mid}$ (19). Combining the secondary structure predictions of Apc1 with structural information from the APC/C atomic model determined using a 3.6-Å resolution cryo-EM map (19), we designed the following Apc1N constructs: $Apc1N^{WT}$, $Apc1N^{\Delta loop2}$, $Apc1N^{\Delta loops2\&3}$, and $Apc1N^{\Delta loops1\&2\&3}$ (Fig. 1*B*). The resultant proteins were expressed using the insect cell/baculovirus system, purified (Fig. S1*A*), and screened for crystallization conditions. The stability of the four Apc1N constructs was examined using thermal shift assays. The combined deletion of loops 1, 2, and 3 ($Apc1N^{\Delta loops1\&2\&3}$) greatly increased the thermal stability of the protein (Fig. S1 *B* and *C*) and allowed its crystallization.

The $Apc1N^{\Delta loops1\&2\&3}$ construct yielded protein crystals that diffracted to 2.2-Å resolution (Table S1). The crystal structure of $Apc1N^{\Delta loops1\&2\&3}$ was determined using the cryo-EM–derived APC/C atomic model (19) as a search object in molecular replacement. The crystal structure of $Apc1N^{\Delta loops1\&2\&3}$ was confirmed as a WD40 β-propeller domain, which consists of seven blades, each with either four or five β-strands (Fig. 1*B* and Fig. S1*D*). The Apc1 WD40 domain ($Apc1^{WD40}$) is ∼70 Å in diameter across its top face and ∼50 Å in height (Fig. 1*B*). In blade 7, an N-terminal β-strand (β7D) joins strands β7A–C to close the propeller in a Velcro-like closure common to β-propeller domains (35). Loop 2, the longest disordered loop, was removed from the segment connecting β-strands β4D and β4E, and loops 1 and 3 were removed from the segments connecting β7D with β1A and β6D with β7A, respectively (Fig. 1*B* and Fig. S1*D*). There is only one helical region in $Apc1^{WD40}$, located within the extended loop that emerges from strand β7D. The WD40 repeat domain is an ancient conserved architecture that functions in many cellular processes (36, 37). The similarities of $Apc1^{WD40}$ to other WD40 domain proteins were assessed using the pairwise structural comparison server DALI (Table S2) (38).

As expected, the $Apc1^{WD40}$ crystal structure is in good agreement with the $Apc1^{WD40}$ model from the cryo-EM structure of APC/C–Cdh1–Emi1 at 3.6 Å (19). The two structures aligned with an rmsd value of 1 Å (Fig. S2*A*). Because the crystal structure is at higher resolution than the cryo-EM structure, it better defines side-chain rotamers (Fig. S2 *B* and *C*), and $Apc1^{WD40}$–water interactions also can be observed.

$Apc1^{WD40}$ Interacts with Apc5 and Apc8B. Within the context of the APC/C assembly, $Apc1^{WD40}$ tucks into the helical groove of

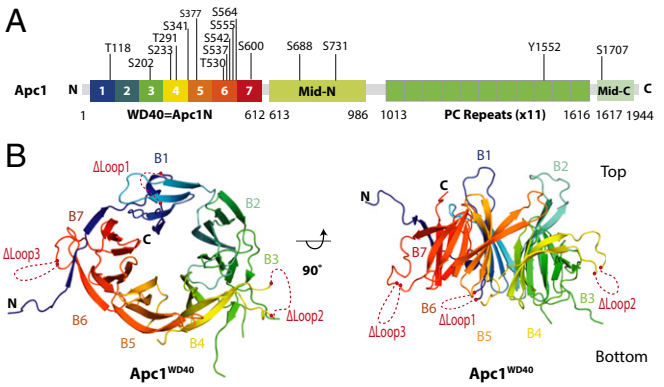

Fig. 1. Crystal structure of $Apc1^{WD40}$. (*A*) Schematic of domain architecture of Apc1. The $Apc1^{WD40}$ β-propeller structure determined in this study is rainbow color-coded. Phosphorylation sites as defined in ref. 19 are indicated. (*B*) Ribbons representation of the Apc1 N-terminal β propeller. Deleted loops are indicated by dashed red lines. Loop 1: residues 34–69; loop 2: residues 307–402; loop 3: residues 523–580.

$Apc5^{TPR}$ (the TPR domain of Apc5) and forms an edge-on contact with the C-terminal TPR helix of Apc8B (one subunit of the homodimer Apc8) (Fig. S3) (12, 19). To gain structural insights into the interactions of $Apc1^{WD40}$ with Apc5 and Apc8B, we mapped the sequence conservation and electrostatic potential of $Apc1^{WD40}$ onto its molecular surface. The surface electrostatic analysis shows that $Apc1^{WD40}$ is predominantly negatively charged, especially on surfaces that interact with complementary positively charged regions of Apc5 and Apc8B (Fig. S3), and, notably, these interacting regions are evolutionarily conserved (Fig. S3 *D* and *E*). The interface interactions between $Apc1^{WD40}$ and Apc5 and Apc8B were analyzed using Protein Interfaces, Surfaces, and Assemblies (PISA) (Table S3). Conformational differences between the crystal and EM structures of $Apc1^{WD40}$, confined mainly to surface loops, accommodate the interaction of $Apc1^{WD40}$ with Apc5 and Apc8B (Fig. S3 *B* and *C*).

$Apc1^{WD40}$ Is Required for APC/C–UbcH10 Ubiquitination Activity. To understand better the function of $Apc1^{WD40}$ for APC/C activity and its contribution to the overall conformation of the APC/C, we reconstituted recombinant mutant APC/C lacking $Apc1^{WD40}$ ($APC/C^{\Delta Apc1-WD40}$) and tested its activity using in vitro ubiquitination assays. As judged by SDS/PAGE gels (Fig. S4*A*) and single-particle negative-stain EM (Fig. 2*A*), $APC/C^{\Delta Apc1-WD40}$ was assembled correctly. Strikingly however, in contrast to wild-type APC/C, the UbcH10-dependent APC/C ubiquitination activity was abolished, even at 30 μM UbcH10 [∼100-fold its K_d (12)] (compare lanes 2–4 with lanes 5–7 in Fig. 2*C*). When the purified $Apc1^{WD40}$ was added back to the $APC/C^{\Delta Apc1-WD40}$, ubiquitination activity was restored (lanes 8–10 in Fig. 2*C*). In addition, the reconstituted $APC/C^{\Delta Apc1-WD40}$–$Apc1^{WD40}$ complex is structurally equivalent to the wild-type PC/C complex as revealed by negative-stain EM (Fig. 2*B*), indicating that the mutant complex activity and structure could be fully recovered by the addition of $Apc1^{WD40}$. Thus, $Apc1^{WD40}$ is essential for APC/C–Cdh1–UbcH10 catalytic activity.

An $Apc1^{WD40}$ Loop Regulates APC/C^{Cdc20} Activity. As discussed above, three disordered loops were deleted from $Apc1^{WD40}$ to aid successful protein crystallization. Numerous mitotic phosphorylation sites are located within these loops, implicating a potential role in regulating Cdc20 interactions with the APC/C. This idea has been confirmed recently by structural and biochemical studies (39, 40). We therefore addressed the requirement of these $Apc1^{WD40}$ loops for APC/C activity. To obtain versions of APC/C lacking one or

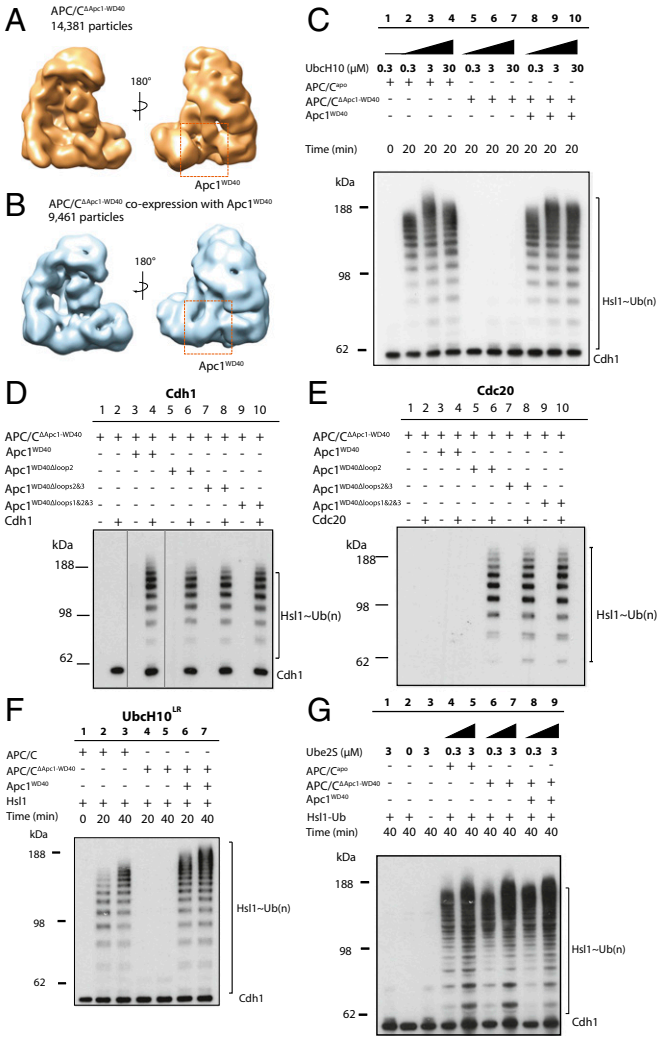

Fig. 2. APC/C$^{\Delta Apc1-WD40}$–Cdh1 is inactive toward UbcH10 but active toward Ube2S. (*A* and *B*) Negative-stain EM reconstructions of APC/C$^{\Delta Apc1-WD40}$ (*A*) and APC/C$^{\Delta Apc1-WD40}$ with coexpressed Apc1^{WD40} (*B*). (*C*) E3 ligase activity of the wild-type APC/C and APC/C$^{\Delta Apc1-WD40}$ with Cdh1, Hsl1, and UbcH10 (lanes 1 to 4). In contrast to wild-type APC/C, APC/C$^{\Delta Apc1-WD40}$–UbcH10 did not ubiquitinate Hsl1 (lanes 5 to 7). Adding back Apc1^{WD40} to APC/C$^{\Delta Apc1-WD40}$ restored activity (lanes 8 to 10). (*D*) Ubiquitination assays of the Cdh1-mediated APC/C$^{\Delta Apc1-WD40\text{-loops}}$ activity. Lanes 1 to 10 correspond to lanes 1, 2, 11, 12, and 5-10 of the original Western blot. This is consistent with the order of lanes in Fig. 2*E*. Lines were added surrounding spliced lanes 3 and 4. As in *C*, APC/C$^{\Delta Apc1-WD40}$–Cdh1 showed no activity compared with apo APC/C$^{\Delta Apc1-WD40}$. The APC/C–Cdh1 ubiquitination activity toward Hsl1 was restored by adding back Apc1^{WD40}, Apc1$^{WD40-\Delta loop2}$, Apc1$^{WD40-\Delta loops2\&3}$, and Apc1$^{WD40-\Delta loops1\&2\&3}$. (*E*) Ubiquitination activity of APC/C$^{\Delta Apc1-WD40}$ with Cdc20 and loop deletions of Apc1^{WD40}. APC/C$^{\Delta Apc1-WD40}$–Cdc20 was not active and could not be activated with wild-type Apc1^{WD40}. The addition of Apc1$^{WD40-\Delta loop2}$, Apc1$^{WD40-\Delta loops2\&3}$, or Apc1$^{WD40-\Delta loops1\&2\&3}$ to APC/C$^{\Delta Apc1}$ allowed APC/C$^{\Delta Apc1}$ to be activated by Cdc20. (*F*) Ubiquitination activity of APC/C–UbcH10^{LR} toward Hsl1. In contrast to wild-type APC/C (lanes 2 and 3), APC/C$^{\Delta Apc1-WD40}$–UbcH10^{LR} did not ubiquitinate Hsl1 (lanes 4 and 5). The addition of Apc1^{WD40} restored the ubiquitination activity (lanes 6 and 7). (*G*) Ubiquitination assay of APC/C$^{\Delta Apc1-WD40}$ with Cdh1, Hsl1–K1–Ub, and Ube2S. APC/C$^{\Delta Apc1-WD40}$–Cdh1 showed higher activity than the wild-type APC/C–Cdh1. The reconstituted APC/C$^{\Delta Apc1-WD40}$–Cdh1–Apc1^{WD40} complex showed activity similar to that of wild-type APC/C.

more Apc1^{WD40} loops, APC/C$^{\Delta Apc1-WD40}$ was reconstituted with individual Apc1^{WD40} loop-deletion constructs. The activity of the resultant reconstituted APC/C was then tested. These tests showed that the catalytic activity of APC/C$^{\Delta Apc1-WD40}$–Cdh1 is restored with any of the Apc1^{WD40} loop-deletion constructs (lanes 4, 6, 8, and 10 in Fig. 2*D*). Therefore the three loops of Apc1^{WD40} are not required for APC/C–Cdh1 catalytic activity. Strikingly, when we used Cdc20 as the coactivator, although APC/C$^{\Delta Apc1-WD40}$ was not activated using wild-type Apc1^{WD40} (lane 4 in Fig. 2*E*), the loop 2 deletion construct of Apc1^{WD40} generated active APC/C^{Cdc20} (lane 6 in Fig. 2*E*). Additional deletions of loops 1 and 3 did not further activate APC/C^{Cdc20} (lanes 8 and 10 in Fig. 2*E*). This result, indicating that loop 2 (residues 307–402) of Apc1^{WD40} inhibits Cdc20 activity, is in agreement with the identification of an autoinhibitory segment within this loop that blocks the binding site of the coactivator C-box on Apc8B (39, 40). Phosphorylation of loop 2 (referred to as the "300s loop" in ref. 39) by mitotic kinases displaces the autoinhibitory segment, relieving the steric blockade of the C-box binding site, thereby permitting APC/C–Cdc20 interactions (39). Thus, deletion of loop 2 of Apc1^{WD40} (also termed the "300s loop") enables APC/C^{Cdc20} activation, mimicking the effects of mitotic APC/C phosphorylation. This finding is in agreement with recent studies (39, 40).

Apc1^{WD40} Is Required for the APC/C–Cdh1 Complex to Bind UbcH10. The loss of APC/C catalytic activity in the absence of Apc1^{WD40} could result from the loss of either UbcH10 or substrate/coactivator interactions with the mutant APC/C. The latter possibility was excluded because an APC/C$^{\Delta Apc1-WD40}$–Cdh1–Hsl1 complex was isolated using size-exclusion chromatography (lane 4 in Fig. S4*B*). To test the association of UbcH10 with both the APC/C and APC/C$^{\Delta Apc1-WD40}$, size-exclusion chromatography was performed. An excess of biotinylated UbcH10, prepared as described (12), was incubated with either wild-type ternary APC/C–Cdh1–Hsl1 or mutant ternary APC/C$^{\Delta Apc1-WD40}$–Cdh1–Hsl1 complexes. Although wild-type ternary APC/C binds UbcH10 (lane 2 in Fig. S4*C*), virtually no UbcH10 coeluted with APC/C$^{\Delta Apc1-WD40}$–Cdh1–Hsl1 (lane 4 in Fig. S4*C*). However, UbcH10 associated with the reconstituted APC/C$^{\Delta Apc1-WD40}$–Cdh1–Hsl1–Apc1^{WD40} complex, as it did with wild-type APC/C (lane 6 in Fig. S4*C*). Thus, Apc1^{WD40} is required for UbcH10 to associate optimally with the APC/C–coactivator complex, and the loss of UbcH10-dependent catalytic activity of the APC/C$^{\Delta Apc1-WD40}$ mutant results (at least in part) from the loss of UbcH10 binding.

UbcH10^{LR} [a fusion of the LR motif of Ube2S (residues 154–222) to the C terminus of UbcH10] has a higher affinity for APC/C than does wild-type UbcH10 because the LR motif of UbcH10^{LR} engages the LR motif-binding site at the interface of Apc2 and Apc4 (12, 19). Using size-exclusion chromatography, we could detect binding of UbcH10^{LR} to both APC/C–Cdh1–Hsl1 and APC/C$^{\Delta Apc1-WD40}$–Cdh1–Hsl1 (lanes 3 and 5 in Fig. S4*B*). However, despite the binding of UbcH10^{LR} to APC/C$^{\Delta Apc1-WD40}$, the mutant APC/C$^{\Delta Apc1-WD40}$–Cdh1 complex was still unable to ubiquitinate Hsl1 (compare lanes 2 and 3 with lanes 4 and 5 in Fig. 2*F*). These data are consistent with the idea that in the APC/C$^{\Delta Apc1-WD40}$–Cdh1 complex the recognition site for the Ubc domain of UbcH10 on the APC/C's catalytic module, necessary to stimulate UbcH10 catalytic activity (19, 20), is not accessible.

Apc1^{WD40} Is Not Required for APC/C–Ube2S Ubiquitination Activity. Although the APC/C$^{\Delta Apc1-WD40}$–Cdh1–UbcH10 E2–E3 pair is deficient in substrate ubiquitination, it remained possible that APC/C$^{\Delta Apc1-WD40}$–Cdh1 might still promote Ube2S-dependent extension of ubiquitin moieties conjugated to APC/C substrates. To address this possibility, we tested whether APC/C$^{\Delta Apc1-WD40}$–Cdh1 could catalyze Ube2S-mediated elongation of an APC/C substrate primed with ubiquitin. We used a modified Hsl1 substrate in which all Lys residues except that in the KEN box were replaced with arginines and a ubiquitin moiety was fused to Hsl1's C terminus (Hsl1–K1–Ub). Interestingly, both wild-type APC/C–Cdh1 (lanes 2 and 3 in Fig. 2*G*) and the mutant

APC/C$^{\Delta Apc1-WD40}$–Cdh1 (lanes 4 and 5 in Fig. 2*G*) ubiquitinated Hsl1–K1–Ub. Surprisingly, APC/C$^{\Delta Apc1-WD40}$ had a slightly higher activity than wild-type APC/C. In conclusion, our results reveal that without Apc1^{WD40} the APC/C$^{\Delta Apc1-WD40}$–Cdh1–Hsl1 complex is impaired in substrate ubiquitination because its ability to bind UbcH10 in a catalytically productive mode is disrupted.

The APC/C$^{\Delta Apc1-WD40}$–Cdh1–Hsl1 Complex Is Locked in the Inactive Conformation. Previous cryo-EM reconstructions of human APC/C revealed that coactivator induces a conformational change of the platform subcomplex and the associated Apc2–Apc11 catalytic module. Additionally, the entire TPR subcomplex rotates relative to Apc1^{PC}. In the presence of coactivator, the catalytic module is shifted to an upward position, away from Apc4 and Apc5 of the platform, thereby exposing the UbcH10-binding sites on Apc11^{RING} and Apc2^{WHB} (Fig. 3 *A* and *B*) (12, 19, 20). In these structures the small subunit Apc15, which is required for Cdc20 autoubiquitination (21–23), adopts an extended conformation anchored to Apc5 by its N terminus and bridging Apc5 and Apc8A through its adjacent N-terminal helix (Apc15^{NTH}) (Fig. 3 *A* and *B*).

To obtain structural insights into the inability of APC/C$^{\Delta Apc1-WD40}$ to ubiquitinate substrates when paired with UbcH10, we determined the cryo-EM structures of both apo APC/C$^{\Delta Apc1-WD40}$ (Fig. 3 *C* and *D*) and a ternary APC/C$^{\Delta Apc1-WD40}$–Cdh1–Hsl1 complex (Fig. 3 *C* and *E*) at 6.0-Å resolution (Fig. S5 *C*–*J*). An atomic model of apo APC/C$^{\Delta Apc1-WD40}$ (Fig. 4*D*) was built by docking models of apo APC/C (39) into the cryo-EM reconstruction. APC/C$^{\Delta Apc1-WD40}$–Cdh1–Hsl1 (Fig. 4*E*) was built using apo APC/C (39) and APC/C–Cdh1–Hsl1–UbcH10 (19) coordinates. Except for the absence of Apc1^{WD40}, the apo states of wild-type APC/C and mutant APC/C$^{\Delta Apc1-WD40}$ are essentially identical (Fig. 4 *A* and *D*).

Strikingly, 3D classification of the APC/C$^{\Delta Apc1-WD40}$–Cdh1–Hsl1 cryo-EM dataset showed that even when associated with coactivator, APC/C particles are locked in the inactive state with the catalytic module occupying the downward position (Figs. 3 *C* and *E* and 4*E*). This APC/C conformation resembles apo APC/C (Fig. 4 *A* and *D*) and is associated with low affinity for UbcH10 and low ubiquitination activity (12). The smaller coactivator-induced rotation of the entire TPR subcomplex relative to Apc1^{PC} is retained in APC/C$^{\Delta Apc1-WD40}$. In the downward conformation, UbcH10 is unable to engage the catalytic module for two reasons. First, docking UbcH10 onto Apc11^{RING}, as observed in the APC/C–Cdh1–substrate–UbcH10 complex (19, 20), shows that UbcH10 would clash with Apc5^{TPR}. Second, in this conformation Apc2^{WHB}, which is required for high-affinity UbcH10 interactions and for stimulating ubiquitin transfer from UbcH10–Ub conjugates (20), would clash with Apc5^{TPR} (see Fig. S7). In contrast to apo APC/C$^{\Delta Apc1-WD40}$ and the ternary APC/C–Cdh1–Hsl1 complex, EM densities corresponding to Apc15 and the N-terminal TPR helix of Apc5^{TPR} are not visible in the APC/C$^{\Delta Apc1-WD40}$–Cdh1–Hsl1 complex (Fig. 3 *D* and *E*), indicating their structural disorder. Size-exclusion chromatography showed that Apc15 dissociated from the APC/C$^{\Delta Apc1-WD40}$–Cdh1–Hsl1 complex (Fig. S5 *A* and *B*).

The disordering of Apc15 and the N-terminal TPR helix of Apc5^{TPR} is a consequence of the Cdh1-induced conformational change of the APC/C that is disrupted in the APC/C$^{\Delta Apc1-WD40}$ mutant by the loss of Apc1^{WD40}. In apo APC/C (wild type and APC/C$^{\Delta Apc1-WD40}$ mutant), Apc8B is well ordered, and its C-terminal TPR motifs interact with the outer α-helices of Apc1^{PC} (Fig. 4 *C* and *F* and Fig. S6) (12, 19). On associating with the APC/C, the N-terminal domain of Cdh1 (Cdh1^{NTD}) interacts both with Apc8B (C-box interaction) and with a site on Apc1^{PC} that overlaps with the Apc1^{PC}–Apc8B interface (Fig. S6) (12, 19). This latter interaction disrupts Apc8B–Apc1^{PC} contacts, resulting in a downward shift of Apc8B's C-terminal TPR motifs. The downward movement of Apc8B pushes simultaneously on the N-terminal TPR helix of Apc5^{TPR} and on Apc1^{WD40}. In turn, movement of Apc1^{WD40} causes a shift of the C-terminal TPR helix of Apc5^{TPR}, resulting in a concerted motion of the whole Apc5^{TPR} domain. The overall effect is that the platform subcomplex rotates, lifting it and the associated catalytic module upward at the front of the molecule into the catalytically active conformation (Fig. 4 *B* and *C*) (12, 19). In APC/C$^{\Delta Apc1-WD40}$–Cdh1–Hsl1, however, because of the loss of Apc1^{WD40}, the downward movement of Apc8B causes a displacement of only the N-terminal TPR helix of Apc5^{TPR}, whereas the C-terminal TPR helix of Apc5^{TPR} remains in the inactive conformation. Motion of the C-terminal TPR helix of Apc5^{TPR} is likely to be the main driving force for rotation of the platform. Thus, with Apc8B pushing down on the N-terminal TPR helix of Apc5^{TPR}, without motion of Apc4 and the C-terminal TPR helix of Apc5^{TPR}, the N-terminal TPR helix of Apc5^{TPR} clashes with Apc8B, distorting the TPR helical geometry; this distortion is likely further accentuated by the noncoordinated motion of the C-terminal TPR helix of Apc5^{TPR} (Fig. S6). Thus the loss of Apc1^{WD40} destabilizes and disorders the N-terminal TPR helix of Apc5^{TPR} and disrupts interactions with the N-terminal extended

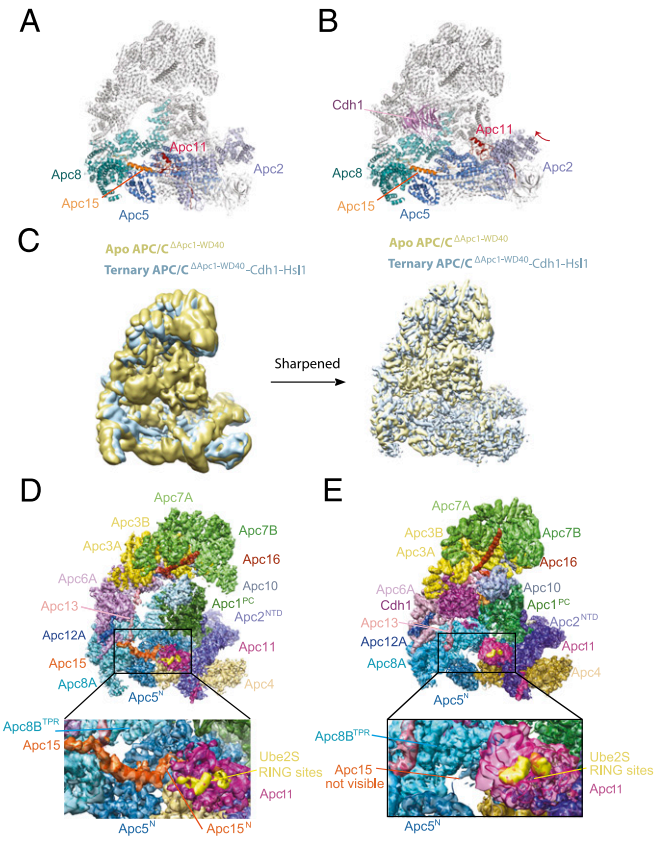

Fig. 3. Cdh1 cannot induce the active conformation of APC/C$^{\Delta Apc1-WD40}$. (*A* and *B*) Ribbon representation of wild-type apo APC/C (*A*) and ternary APC/C–Cdh1–Hsl1 complex (*B*). These two structures show the coactivator-induced conformational change of the catalytic module of Apc2–Apc11. (*C*) Superimposition of the 6-Å resolution cryo-EM maps of apo APC/C$^{\Delta Apc1-WD40}$ (yellow) and the ternary APC/C$^{\Delta Apc1-WD40}$–Cdh1–Hsl1 complex (light blue). (*D*) View of the apo APC/C$^{\Delta Apc1-WD40}$ molecular envelope with the EM maps color-coded according to subunit assignments. (*E*) View of the ternary APC/C$^{\Delta Apc1-WD40}$–Cdh1–Hsl1 EM map. The EM density for Apc15 seen in *D* is not visible.

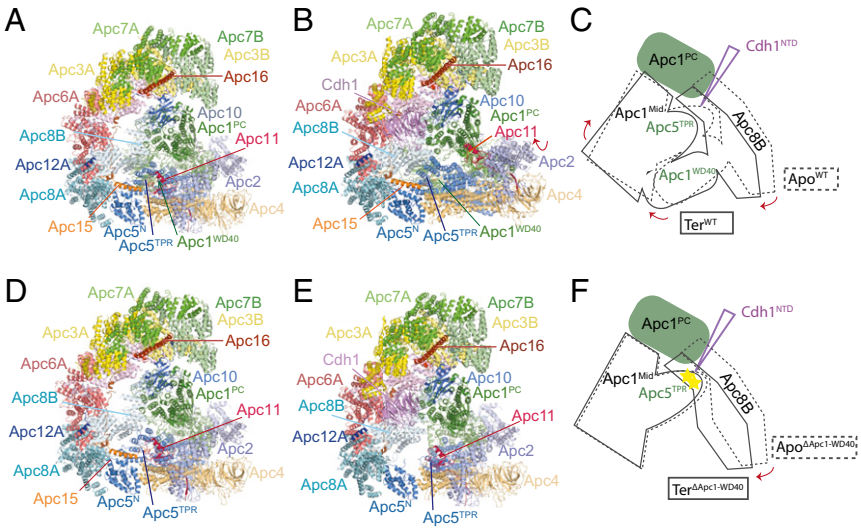

Fig. 4. Comparison of apo APC/C$^{\Delta Apc1-WD40}$ and ternary APC/C$^{\Delta Apc1-WD40}$–Cdh1–Hsl1 complexes with wild-type APC/C. (*A*) Apo APC/C. (*B*) Ternary APC/C–Cdh1–Hsl1. (*C*) Schematic of the conformational change on conversion from the apo to the ternary state. The N-terminal domain of Cdh1 (Cdh1^{NTD}) acts as a wedge to separate Apc1^{PC} from Apc8B. Apc8B is pushed down on Apc5^{TPR} and Apc1^{WD40}, shifting Apc4 and causing the platform subcomplex to rotate. (*D*) Apo APC/C$^{\Delta Apc1-WD40}$. (*E*) Ternary APC/C$^{\Delta Apc1-WD40}$–Cdh1–Hsl1. (*F*) Schematic of the conformational change on conversion from the apo to the ternary state. Apc8B pushes down on Apc5^{TPR}; however, because of the absence of Apc1^{WD40}, the conformational changes are not transmitted to Apc4; the platform remains unchanged, and the N-terminal domain of Apc5^{TPR} becomes distorted, destabilizing its contacts with the N terminus of Apc15, which dissociates.

segment of Apc15 that is responsible for anchoring Apc15 to Apc5 (Fig. 3*D*).

Interestingly, the conformation of APC/C$^{\Delta Apc1-WD40}$–Cdh1–Hsl1 resembles the hybrid class observed in the EM datasets of wild-type ternary APC/C–coactivator–substrate complexes (~10% of APC/C particles) (12, 19, 39). In the hybrid state, the catalytic module adopts the inactive conformation, and EM densities for Apc1^{WD40} and Apc15 are absent. We assume that the hybrid state results from an N-terminal truncation of a minor portion of Apc1 during expression and purification of the recombinant APC/C (Figs. S4*B* and S5*A*).

Discussion

In this study we have used information from a cryo-EM model to determine the crystal structure of Apc1^{WD40} at higher resolution, highlighting the complementarity of X-ray crystallography and cryo-EM. Our results reveal that, in the absence of Apc1^{WD40}, the APC/C$^{\Delta Apc1-WD40}$–Cdh1–Hsl1 complex is locked in the inactive conformation with the Apc2^{CTD}–Apc11^{RING} catalytic module positioned in the downward conformation. Thus, Apc1^{WD40} functions to stabilize the active conformation of the APC/C but is not required to stabilize the inactive conformation.

The inability of APC/C$^{\Delta Apc1-WD40}$ to adopt the active conformation results in a loss of catalytic activity of the APC/C$^{\Delta Apc1-WD40}$–Cdh1–UbcH10 E3–E2 pair because UbcH10 is unable to engage APC/C's catalytic module. However, this inactive conformation did not affect the ability of Ube2S to assemble a polyubiquitin chain on Hsl1–K1–Ub. This finding indicates that, although coactivators regulate the catalytic activity of the APC/C toward the priming E2 (UbcH10) through a conformational change that renders the UbcH10-binding site on the catalytic module accessible, the intrinsic catalytic activity of the APC/C–Ube2S pair is independent of coactivator. Unlike UbcH10, the affinity of Ube2S for the APC/C is not dependent on coactivator (12). Ube2S interacts with the APC/C through its C-terminal LR tail at the interface of Apc2–Apc4 (19) and interacts with Apc2 through its Ubc catalytic domain (31). This LR tail-binding site does not change conformation on interconversion between active and inactive states (12, 39). Although independent of the catalytic module for APC/C binding, the catalytic activity of Ube2S requires the RING domain of Apc11 that is repurposed to engage the acceptor ubiquitin of the APC/C substrate for covalent linkage with the donor ubiquitin of the Ube2S–ubiquitin conjugate (14, 30). The acceptor ubiquitin-binding site on Apc11 is accessible in the inactive APC/C conformation (Fig. 3 *D* and *E*) as is consistent with our findings that Ube2S extends ubiquitin on the Hsl1–K1–Ub substrate in the context of the APC/C$^{\Delta Apc1-WD40}$–Cdh1–Hsl1–Ub complex. This study shows that, similar to the affinity of Ube2S for the APC/C (19), the catalytic activity of Ube2S in complex with the APC/C is not stimulated by the coactivator-induced conformational changes within the APC/C.

The affinity of apo APC/C for UbcH10 is four- to eightfold lower than for the ternary APC/C–Cdh1–substrate complex (12). However, the present study indicates that the inactive conformation adopted by apo APC/C would be incapable of engaging UbcH10. We suggest that the APC/C interconverts between an inhibited conformation that is unable to bind UbcH10 and an active conformation that binds UbcH10 even in the absence of coactivator. This interconversion would explain the capacity of apo APC/C to bind UbcH10 with low affinity, the small but detectable binding of UbcH10 to APC/C$^{\Delta Apc1-WD40}$–Cdh1–Hsl1 (Fig. S4*C*), and the low ubiquitination activity of APC/C$^{\Delta Apc1-WD40}$ (Fig. 2*D*). Analysis of 3D classes of apo wild-type APC/C and mutant APC/C$^{\Delta Apc1-WD40}$ EM datasets indicates a small population of molecules (roughly 8%) in which the catalytic module (Apc2^{CTD}–Apc11) adopts an upward conformation because of rotation about the Apc2^{CTD}–Apc2^{NTD} interface, with the platform remaining in the inactive conformation (Fig. S7 *C* and *D*). This upward conformation of the catalytic module would allow binding of UbcH10 to Apc11^{RING} and Apc2^{WHB} (Fig. S7 *E* and *F*).

It is interesting to consider the possibility that controlling the association of Apc1^{WD40} with its binding pocket in the APC/C could provide a potential regulatory mechanism. Thus, proteins that bind to Apc1^{WD40} and compete for its association with its docking site on the APC/C would displace Apc1^{WD40}, thereby inactivating the APC/C. The APC/C$^{\Delta Apc1-WD40}$ mutant has unexpectedly provided a system for exploring the different ubiquitination mechanisms of human APC/C with its two cognate E2s UbcH10 and Ube2S.

Materials and Methods

X-ray data were collected at the Diamond Light Source beamline I02 using a Pilatus 6M-F silicon pixel detector and were processed using XDS (41) and scaled using Aimless (42) in the CCP4i software package (43, 44). Cryo-EM data were collected using a 300-kV FEI Polara electron microscope and were processed using the RELION (Regularized Likelihood Optimization) software package (45). Detailed procedures for the protein preparation, ubiquitination assays, crystallization, and EM data processing are provided in *SI Materials and Methods*.

ACKNOWLEDGMENTS. We thank members of the D.B. group for discussion and reagents; C. Savva, S. Chen, and G. McMullan for help with EM data collection; X. Bai and K. Zhang for help with EM data analysis; J. Grimmet and T. Darling for computing; A. Boland, M. Yu, and G. Murshudov for advice and help with X-ray data collection, processing, and analysis; the staff at Diamond Light Source for help with data collection; and C. Alfieri for advice and comments on the manuscript. Recombinant Cdc20 was a generous gift of S. Zhang. This work was supported by a grant from the Cancer Research-UK Programme Grant C576/A14109 (to D.B.) and the Medcal Research Council Laboratory of Molecular Biology (MRC_UP_1201/6). Q.L. is the recipient of an Institute of Cancer Research Studentship.

1. Morgan DO (2006) *The Cell Cycle: Principles of Control*, Primers in Biology (New Science Press, London).
2. Hunt T, Nasmyth K, Novák B (2011) The cell cycle. *Philos Trans R Soc Lond B Biol Sci* 366(1584):3494–3497.
3. Wieser S, Pines J (2015) The biochemistry of mitosis. *Cold Spring Harb Perspect Biol* 7(3):a015776.
4. Peters JM (2006) The anaphase promoting complex/cyclosome: A machine designed to destroy. *Nat Rev Mol Cell Biol* 7(9):644–656.
5. Pines J (2011) Cubism and the cell cycle: The many faces of the APC/C. *Nat Rev Mol Cell Biol* 12(7):427–438.
6. Barford D (2011) Structure, function and mechanism of the anaphase promoting complex (APC/C). *Q Rev Biophys* 44(2):153–190.
7. Meyer HJ, Rape M (2011) Processive ubiquitin chain formation by the anaphase-promoting complex. *Semin Cell Dev Biol* 22(6):544–550.
8. Primorac I, Musacchio A (2013) Panta rhei: The APC/C at steady state. *J Cell Biol* 201(2): 177–189.
9. Sivakumar S, Gorbsky GJ (2015) Spatiotemporal regulation of the anaphase-promoting complex in mitosis. *Nat Rev Mol Cell Biol* 16(2):82–94.
10. Bochis OV, Fetica B, Vlad C, Achimas-Cadariu P, Irimie A (2015) The importance of ubiquitin E3 ligases, SCF and APC/C, in human cancers. *Clujul Med* 88(1):9–14.
11. Kimata Y, Baxter JE, Fry AM, Yamano H (2008) A role for the Fizzy/Cdc20 family of proteins in activation of the APC/C distinct from substrate recruitment. *Mol Cell* 32(4): 576–583.
12. Chang L, Zhang Z, Yang J, McLaughlin SH, Barford D (2014) Molecular architecture and mechanism of the anaphase-promoting complex. *Nature* 513(7518):388–393.
13. Van Voorhis VA, Morgan DO (2014) Activation of the APC/C ubiquitin ligase by enhanced E2 efficiency. *Curr Biol* 24(13):1556–1562.
14. Kelly A, Wickliffe KE, Song L, Fedrigo I, Rape M (2014) Ubiquitin chain elongation requires E3-dependent tracking of the emerging conjugate. *Mol Cell* 56(2):232–245.
15. Jörgensen PM, et al. (2001) Characterisation of the human APC1, the largest subunit of the anaphase-promoting complex. *Gene* 262(1-2):51–59.
16. He J, et al. (2012) The structure of the 26S proteasome subunit Rpn2 reveals its PC repeat domain as a closed toroid of two concentric α-helical rings. *Structure* 20(3): 513–521.
17. Steen JA, et al. (2008) Different phosphorylation states of the anaphase promoting complex in response to antimitotic drugs: A quantitative proteomic analysis. *Proc Natl Acad Sci USA* 105(16):6069–6074.
18. Kraft C, et al. (2003) Mitotic regulation of the human anaphase-promoting complex by phosphorylation. *EMBO J* 22(24):6598–6609.
19. Chang L, Zhang Z, Yang J, McLaughlin SH, Barford D (2015) Atomic structure of the APC/C and its mechanism of protein ubiquitination. *Nature* 522(7557):450–454.
20. Brown NG, et al. (2015) RING E3 mechanism for ubiquitin ligation to a disordered substrate visualized for human anaphase-promoting complex. *Proc Natl Acad Sci USA* 112(17):5272–9.
21. Mansfeld J, Collin P, Collins MO, Choudhary JS, Pines J (2011) APC15 drives the turnover of MCC-CDC20 to make the spindle assembly checkpoint responsive to kinetochore attachment. *Nat Cell Biol* 13(10):1234–1243.
22. Foster SA, Morgan DO (2012) The APC/C subunit Mnd2/Apc15 promotes Cdc20 autoubiquitination and spindle assembly checkpoint inactivation. *Mol Cell* 47(6): 921–932.
23. Uzunova K, et al. (2012) APC15 mediates CDC20 autoubiquitylation by APC/C(MCC) and disassembly of the mitotic checkpoint complex. *Nat Struct Mol Biol* 19(11): 1116–1123.
24. Yu H, King RW, Peters JM, Kirschner MW (1996) Identification of a novel ubiquitin-conjugating enzyme involved in mitotic cyclin degradation. *Curr Biol* 6(4):455–466.
25. Jin L, Williamson A, Banerjee S, Philipp I, Rape M (2008) Mechanism of ubiquitin-chain formation by the human anaphase-promoting complex. *Cell* 133(4):653–665.
26. Williamson A, et al. (2011) Regulation of ubiquitin chain initiation to control the timing of substrate degradation. *Mol Cell* 42(6):744–757.
27. Garnett MJ, et al. (2009) UBE2S elongates ubiquitin chains on APC/C substrates to promote mitotic exit. *Nat Cell Biol* 11(11):1363–1369.
28. Williamson A, et al. (2009) Identification of a physiological E2 module for the human anaphase-promoting complex. *Proc Natl Acad Sci USA* 106(43):18213–18218.
29. Wu T, et al. (2010) UBE2S drives elongation of K11-linked ubiquitin chains by the anaphase-promoting complex. *Proc Natl Acad Sci USA* 107(4):1355–1360.
30. Brown NG, et al. (2014) Mechanism of polyubiquitination by human anaphase-promoting complex: RING repurposing for ubiquitin chain assembly. *Mol Cell* 56(2): 246–260.
31. Brown NG, et al. (2016) Dual RING E3 Architectures Regulate Multiubiquitination and Ubiquitin Chain Elongation by APC/C. *Cell* 165(6):1440–1453.
32. Meyer HJ, Rape M (2014) Enhanced protein degradation by branched ubiquitin chains. *Cell* 157(4):910–921.
33. Rodrigo-Brenni MC, Morgan DO (2007) Sequential E2s drive polyubiquitin chain assembly on APC targets. *Cell* 130(1):127–139.
34. Rodrigo-Brenni MC, Foster SA, Morgan DO (2010) Catalysis of lysine 48-specific ubiquitin chain assembly by residues in E2 and ubiquitin. *Mol Cell* 39(4):548–559.
35. Chaudhuri I, Söding J, Lupas AN (2008) Evolution of the beta-propeller fold. *Proteins* 71(2):795–803.
36. Smith TF, Gaitatzes C, Saxena K, Neer EJ (1999) The WD repeat: A common architecture for diverse functions. *Trends Biochem Sci* 24(5):181–185.
37. Xu C, Min J (2011) Structure and function of WD40 domain proteins. *Protein Cell* 2(3): 202–214.
38. Holm L, Rosenstrom P (2010) Dali server: Conservation mapping in 3D. *Nucleic Acids Res* 38(Web Server issue):W545–549.
39. Zhang S, et al. (2016) Molecular mechanism of APC/C activation by mitotic phosphorylation. *Nature* 533(7602):260–264.
40. Qiao R, et al. (2016) Mechanism of APC/CCDC20 activation by mitotic phosphorylation. *Proc Natl Acad Sci USA* 113(19):E2570–E2578.
41. Kabsch W (2010) Xds. *Acta Crystallogr D Biol Crystallogr* 66(Pt 2):125–132.
42. Evans PR (2011) An introduction to data reduction: Space-group determination, scaling and intensity statistics. *Acta Crystallogr D Biol Crystallogr* 67(Pt 4):282–292.
43. Winn MD, et al. (2011) Overview of the CCP4 suite and current developments. *Acta Crystallogr D Biol Crystallogr* 67(Pt 4):235–242.
44. Cowtan K, Emsley P, Wilson KS (2011) From crystal to structure with CCP4. *Acta Crystallogr D Biol Crystallogr* 67(Pt 4):233–234.
45. Scheres SH (2012) RELION: Implementation of a Bayesian approach to cryo-EM structure determination. *J Struct Biol* 180(3):519–530.
46. Zhang Z, Yang J, Barford D (2016) Recombinant expression and reconstitution of multiprotein complexes by the USER cloning method in the insect cell-baculovirus expression system. *Methods* 95:13–25.
47. Zhang Z, et al. (2013) Recombinant expression, reconstitution and structure of human anaphase-promoting complex (APC/C). *Biochem J* 449(2):365–371.
48. McCoy AJ, et al. (2007) Phaser crystallographic software. *J Appl Cryst* 40(Pt 4):658–674.
49. Emsley P, Lohkamp B, Scott WG, Cowtan K (2010) Features and development of Coot. *Acta Crystallogr D Biol Crystallogr* 66(Pt 4):486–501.
50. Adams PD, et al. (2010) PHENIX: A comprehensive Python-based system for macromolecular structure solution. *Acta Crystallogr D Biol Crystallogr* 66(Pt 2):213–221.
51. Murshudov GN, Vagin AA, Dodson EJ (1997) Refinement of macromolecular structures by the maximum-likelihood method. *Acta Crystallogr D Biol Crystallogr* 53(Pt 3): 240–255.
52. Brünger AT, Kuriyan J, Karplus M (1987) Crystallographic R factor refinement by molecular dynamics. *Science* 235(4787):458–460.
53. Chen VB, et al. (2010) MolProbity: All-atom structure validation for macromolecular crystallography. *Acta Crystallogr D Biol Crystallogr* 66(Pt 1):12–21.
54. Baker NA, Sept D, Joseph S, Holst MJ, McCammon JA (2001) Electrostatics of nanosystems: Application to microtubules and the ribosome. *Proc Natl Acad Sci USA* 98(18): 10037–10041.
55. Celniker G, et al. (2013) ConSurf: Using evolutionary data to raise testable hypotheses about protein function. *Isr J Chem* 53(3-4):199–206.
56. UniProt Consortium (2015) UniProt: A hub for protein information. *Nucleic Acids Res* 43(Database issue):D204–D212.
57. Larkin MA, et al. (2007) Clustal W and Clustal X version 2.0. *Bioinformatics* 23(21): 2947–2948.
58. Krissinel E, Henrick K (2007) Inference of macromolecular assemblies from crystalline state. *J Mol Biol* 372(3):774–797.
59. Tang G, et al. (2007) EMAN2: An extensible image processing suite for electron microscopy. *J Struct Biol* 157(1):38–46.
60. Ludtke SJ, Baldwin PR, Chiu W (1999) EMAN: Semiautomated software for high-resolution single-particle reconstructions. *J Struct Biol* 128(1):82–97.
61. Mindell JA, Grigorieff N (2003) Accurate determination of local defocus and specimen tilt in electron microscopy. *J Struct Biol* 142(3):334–347.
62. Scheres SH (2015) Semi-automated selection of cryo-EM particles in RELION-1.3. *J Struct Biol* 189(2):114–122.
63. Scheres SH, Chen S (2012) Prevention of overfitting in cryo-EM structure determination. *Nat Methods* 9(9):853–854.
64. Bai XC, Fernandez IS, McMullan G, Scheres SH (2013) Ribosome structures to near-atomic resolution from thirty thousand cryo-EM particles. *eLife* 2:e00461.
65. Scheres SH (2014) Beam-induced motion correction for sub-megadalton cryo-EM particles. *eLife* 3:e03665.
66. Yang Z, et al. (2012) UCSF Chimera, MODELLER, and IMP: An integrated modeling system. *J Struct Biol* 179(3):269–278.